



# VLASS Project Memo #19

# An Evaluation of Calibrator Spatial Models in VLASS Single Epoch Calibration

**John J. Tobin, Amy Kimball**

**March 20, 2024**

**Abstract**

We present a feasibility study regarding the use of calibrator spatial models with the VLASS Calibration pipeline. We review the problem of resolved calibrators used within the VLASS survey and how calibrators that may require a spatial model are identified. We then select several VLASS tiles to further examine the impact of a spatial model in their standard calibration. We outline how we created the calibrator spatial model, how we calibrated the data with the spatial model, the places in the pipeline that would need to write the spatial model to a measurement set, and we examine the impact of the spatial model on the resultant images (visually and quantitatively using source catalogs generated from the images). We find that there is little visual impact on the source morphologies in the images nor are there scientifically relevant impacts on the source catalogs created from images that use a spatial model relative to those that did not. *We conclude that in the specific case of the calibrators used for the VLASS survey (i.e., these results are not generally applicable for any resolved calibrator), spatial models are not required to meet the science goals of the survey and we do not recommend that the survey perform special processing on the data previously suggested to require a calibrator spatial model.*

## 1 Introduction

As an all sky survey, one of the challenges that VLASS has dealt with is the availability of calibration sources that are within acceptable angular separations from VLASS tile centers (VLASS Memo #7). While the sky is filled with bright radio sources at S-band (∼3 GHz), many are not ideal complex gain calibration sources. An ideal complex gain calibrator is unresolved, meaning that its amplitude will be constant for all sampled *uv*-distances at a given frequency. This enables the phase and amplitude gain solutions to be computed correctly when an *a priori* spatial model is not available, as is the case for most radio sources.

The VLA calibrator catalog has a large number of bright radio sources; however, it predates the EVLA. As such, there are no S-band entries and there can be inaccuracies in the tabulated data. For example, many sources are resolved at short baselines and this fact is not always indicated in the calibrator catalog. This situation resulted in the first epoch of VLASS using

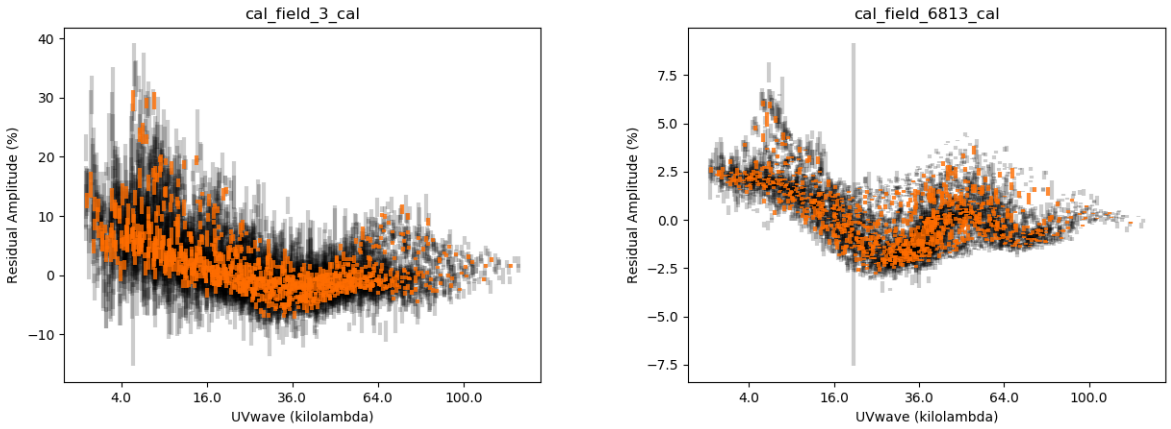


Figure 1: Plot of the residual amplitude vs. *uv*-distance for the two most extreme resolved VLASS calibrators observed in VLASS Epoch 1.1 for Tile T08t07 (J0412+001, left) and T08t10 (J0607−0834, right). The structure is indicative of multiple point sources.

many sub-optimal calibrators that have resolved structure, and the first half epoch (VLASS 1.1) having the largest number of calibrators with resolved structure. The problem has been mitigated with S-band C-config observations of potential VLASS calibrators, and with the ability to use *uv*-ranges in the calibration pipeline. Nonetheless, there are certain VLASS tiles that did not have a point source calibrator available and had to make use of a resolved calibrator in subsequent VLASS epochs. The purpose of this memo is to describe a path to create calibrator models, integrate those models into the calibration pipeline, and assess the impact of the calibrator model on the data. We will detail how the project defines if a model may be needed, our methodology of model creation, including the model in the measurement sets for calibration, and the impact of using the model on images with Quicklook images, which do not include self-calibration, and the Single Epoch images, which include self-calibration on the observed image.

# 2 Determination of when a Calibrator Model is Needed

The calibrators used in each VLASS observation are characterized as part of the VLASS utilities developed by J. Marvil. For each calibrator, the fractional deviation from a constant point source is measured as a function of *uv*-distance. If a resolved calibrator has variations $> \pm 3\%$ at baselines shorter than 35 k$\lambda$ and/or at baselines longer than 90 k$\lambda$, a *uv*-range selection can be used during calibration to avoid including the resolved structure. However, calibrators that have variations $> \pm 3\%$ in the range between 35 to 90 k$\lambda$ have been thought to need a calibrator model. These datasets are processed as normal for VLASS Quicklook images, but have been put on-hold for Single Epoch calibration and imaging. Examples of calibrators with well-resolved structure are shown in Figure 1.

Despite the concern that a >3% deviation of the amplitude vs. *uv*-distance would require a calibrator model, VLASS observations that used resolved calibrators have not been shown to absolutely require a model to obtain scientifically reliable measurements. Therefore we aim to

test the hypothesis that these datasets require a calibrator model for proper calibration.

# 3 Test Procedure

Three main tasks comprised our test procedure:

1. Create a model for the calibrator,
2. Calibrate the data using the calibrator model, and
3. Compare and contrast image data with and without the model applied.

We describe these tasks in greater detail in the following sections. We first needed to select appropriate datasets to characterize the impact of using a calibrator model. The VLASS tiles thought to require a model had already been assessed as part of the VLASS calibration Quality Assurance (QA) procedure. Then from this list of tiles, we examined the plots of residual vs. uv-distance (Figure 1, e.g.) and selected those with the the most egregious resolved calibrator structure. The examples shown in Figure 1 have the most resolved structure in all of VLASS Epoch 1. We list all the VLASS Tiles, Epoch, and resolved calibrators that we used for this investigation in Table 1.

Table 1. Tile List

| Tile | Epoch | Calibrator | Image Types Tested |
|---|---|---|---|
| T08t07 | 1.1 | J0412+0010 | SE, QL |
| T08t10 | 1.1 | J0607-0834 | SE, QL |
| T04t34 | 1.1 | W2300-2644 | SE, QL |
| T14t15 | 1.1 | J0954+1743 | SE, QL |
| T13t13 | 2.1 | J0758+1136 | SE |
| T13t15 | 2.1 | J0946+1017 | SE |

## 3.1 Creation of the Calibrator Model

The creation of a calibrator model is an important piece to this investigation because the spatial model will impact the phase and amplitude gain solutions. Ideally, we would observe the calibrator as a science target and have it phase referenced to a point source calibrator and further self-calibrate the source. However, we are instead using the data from the VLASS observations themselves to create the model. There are cases where the same resolved calibrator is observed for multiple VLASS tiles, which could enable the creation of a better model, if the source is not variable. However, for the purposes of this test, we are only using the calibrator data from the same Execution Block we are testing.

We started the calibrator model creation process using the VLASS data that were calibrated as part of the normal pipeline execution. This first run with the standard calibration pipeline produces the data which we will use to assess the impact of a calibrator model as well as the casa_commands.log file that we will use later to perform the calibration with the calibrator model.

At the end of a pipeline run, the calibrator data has scan-averaged phase and amplitude gain solutions applied to it, which were calculated under the assumption that the calibrator

was a point source. We assumed that starting with a point source model is not completely incorrect and that we could make an improved source model using self-calibration. Indeed, resolved structure is often apparent in the calibrator model images from standard calibration.

We self-calibrated the calibrator sources using a typical self-calibration loop where we start off with scan-averaged solutions, cleaning shallowly, and then cleaning deeper with each successive solution interval while reducing the solution timescale with each self-calibration loop. We solved for both phase and amplitude gains on each solution interval, using the *gaincal* parameter *solnorm = True* to avoid introducing significant changes to the flux density scale. Solving for the phase and amplitude gains simultaneously on each solution interval tended to yield a superior calibrator image than first executing phase-only self-calibration and then performing amplitude self-calibration at the end. We also did not combine spectral windows or polarizations in the computation of the gain solutions used for model creation.

The self-calibration loop was controlled using a semi-automated routine that was based on the prototype used for the CASA pipeline implementation of self-calibration for VLA and ALMA data[1]. However, given the specific use-case of VLASS calibrators that have high S/N, several simplifying assumptions could be made. We always solved on a per-spectral window basis, calculating solutions per polarization, and the calibrator flux densities were high enough that self-calibration could safely be conducted on solution intervals as short as a single integration. We also made use of static masks on the source structure, but upon completion of self-calibration, we would evaluate whether an expanded mask was necessary and—if so—re-run the entire procedure using the final (expanded) mask.

We show an example of the calibrator model for J0607−0834 determined from VLASS data in Figure 2, demonstrating that we are able to construct source models that were reasonable from this method. We did not further explore refinements to the model creation parameter space, but additional optimization of this procedure could yield further improvements to the calibrator models.

With a reasonable spatial model for the calibrator in-hand, we then needed to make use of this model in calibration. For the purposes of these tests, we made use of the *calimage.model.tt0* and *calimage.model.tt1* images from *tclean*. These images contain respectively the absolute flux density and spectral information for the calibrator on a per-pixel basis. We do, however, note that the flux density calibration of this calibrator was performed using gain solutions that assumed a point-source calibrator model. Moreover, the flux density bootstrapping calculates the spectral index for the calibrator using all the emission, not accounting for the fact that different components in the image might have different spectral indices. For example, the point source could have a flat spectrum while a jet knot could have a negative spectral index. Thus, there may be some inaccuracy in the spectral indices of individual model components, but it should be reasonable for the source on the whole. This issue is unavoidable without conducting separate observations using an independent complex gain calibrator.

We expect that it should be possible to renormalize the *calimage.model.tt0* image to 1.0, and allow the pipeline task *hifv_fluxboot* and the CASA task *fluxscale* to determine the spectral index. Then the *calimage.model.tt0* image could be scaled to the fitted flux density and a *calimage.model.tt1* image could be created from it. However, for use in operations it may be more desirable to convert the *calimage.model.tt0* image to a component list and then set the

[1]https://github.com/jjtobin/auto_selfcal

spectral indices of the components. The model column in the measurement set (MS) would then need to be filled via the CASA task *ft* rather than *tclean*, as we used in this exploration; see more details in Section 3.2.

Finally, we did not always choose the calibrator model from the final self-calibration solution interval of solint='int'. We instead sometimes chose the calibrator model from a solution interval that was slightly longer (0.9s or 1.35s). We chose these models because in the later solution intervals, it appeared that *tclean* was cleaning too deeply into the noise and putting some negative components into the model image. The main features of the calibrator emission structure were consistent between the longer solution interval and the solint='int' solution interval. The negative components are not physical and it is advantageous to avoid including too many of them in the calibrator model; however, negative components are at such a low level compared to the positive components that their inclusion would not likely impact the calibration. Future investigations could consider modifications to the clean depth in high dynamic range cases such as these and removing model components that have a tt0 flux density that are below some threshold, which would also implicitly remove the negative model components.

## 3.2 Calibration with the Calibrator Model

We performed a pipeline-assisted calibration to perform the calibration with the calibrator spatial model. We used the standard VLA pipeline script for part of the calibration process, except that we inserted model-writing commands at certain points of the process. In the script shown below, we define a function *run_tclean_cal_model* which writes the *tclean* model image to the model column of the selected MS. We write to the main MS following *hifv_setjy* and prior to *hifv_fluxboot* we write the model to calibrators.ms, which is created during *hifv_solint*. Standard flux density bootstrapping assumes a point source model with a flux of 1.0 Jy and a spectral index of 0, and the bootstrapped calibrator flux density and spectral index are computed relative to this model. However, since we have supplied a model with both absolute flux density information and spectral index (in the form of the tt1 image), no scaling is needed to put the modeled calibrator on an absolute flux density scale. Thus, *hifv_fluxboot* was expected to report a flux density of $\sim$1.0 and a spectral index of $\sim$0.

For much of the remaining pipeline, we also need to replace the pipeline calls with the manual CASA commands. We used the commands listed in the casa_commands.log file produced from the standard pipeline run that did not use a calibrator model. This is necessary because *hifv_finalcals* creates another split MS, finalcalibrators.ms, where we need to also write the calibrator model to its model column such that it can be used for all subsequent calls to *gaincal*. The only remaining pipeline tasks that run successfully are *hifv_statwt* and *hifv_checkflag*. The end result is a calibrated and flagged MS that made use of the specified calibrator model in the calculation of the complex gain solutions. An abbreviated calibration script is included below.

```
context = h_init()
context.set_state("ProjectSummary", "proposal_code", "VLASS")
context.set_state("ProjectSummary", "observatory", "Karl G. Jansky Very Large Array")
context.set_state("ProjectSummary", "telescope", "EVLA")
context.set_state("ProjectSummary", "piname", "unknown")
context.set_state("ProjectSummary", "proposal_title", "unknown")
context.set_state("ProjectStructure", "ppr_file", "PPR.xml")
vis="VLASS2.1.sb38608477.eb38643773.59104.940213009264.ms"

def run_tclean_cal_model(vis, imagename,field="", datacolumn="data", scales=[0],
```

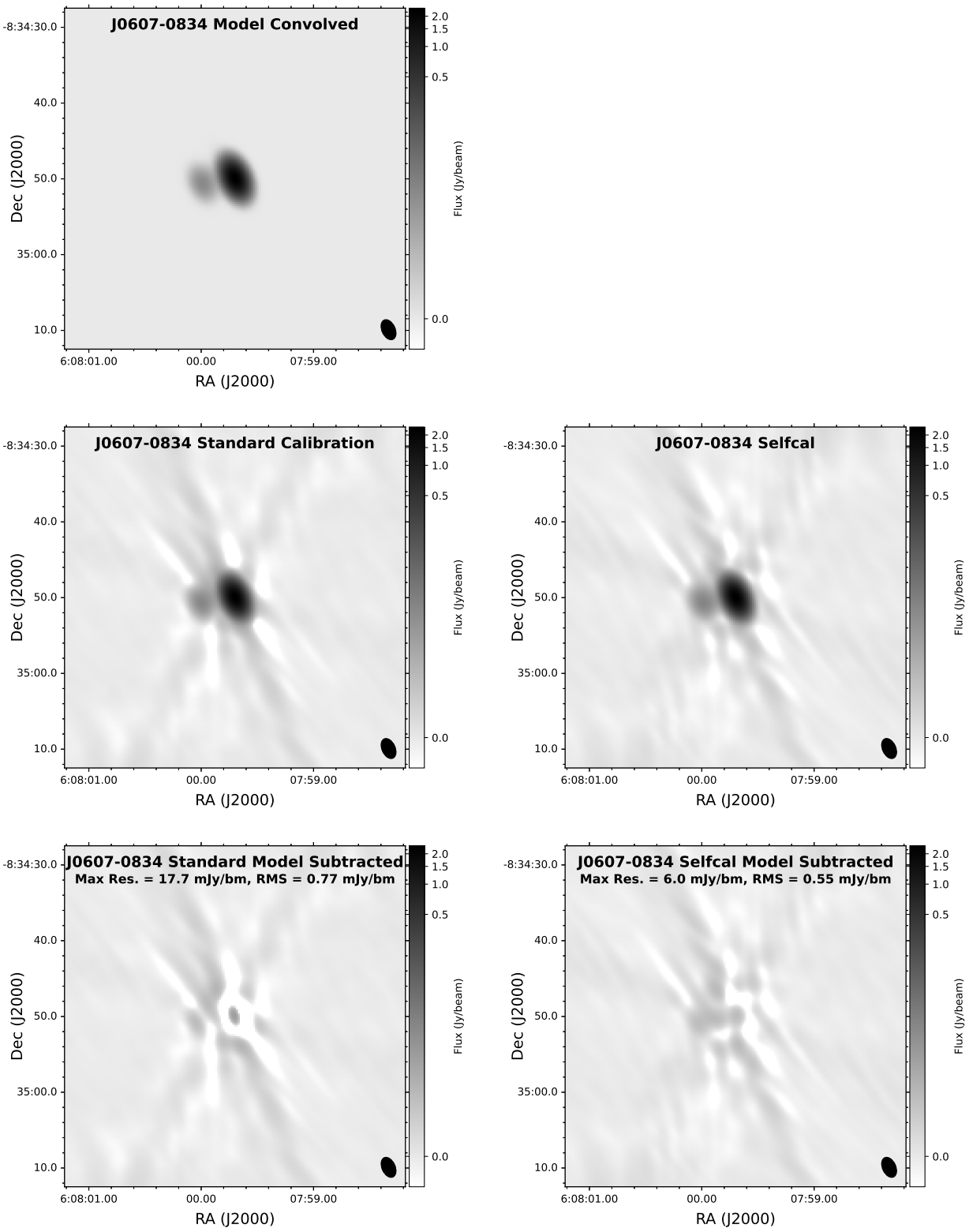


Figure 2: Images of calibrator J0607−0834 (same as the calibrator shown in the right panel of Figure 1). The top row shows the convolved calibrator model constructed using self-calibration. The middle row shows deconvolved images of the calibrator from the standard calibration (left) and self-calibration down to 1.35s (right). The bottom row shows residuals of the convolved model subtracted from the standard calibrated data (left) and the self-calibrated data (right). Stats overlaid on the residual images demonstrate that the self-calibrated image has lower peak and RMS residuals. The peak intensity of the brighter component is 2.4 Jy and the fainter component is 0.035 Jy (68× fainter).

```
    robust=0.5, uvtaper="", niter=0, gain=0.1, nsigma=2.0, cycleniter=500,
    cyclefactor=3, mask="", savemodel="none", calcres=True, calcpsf=True,
    parallel=True,  usemask="user" ,pbmask=0.0,stokes="I",reffreq="3.0GHz",
    spw="",imsize=300,cell="0.25arcsec" ):
    tclean(vis=vis, field=field, spw=spw, uvrange="", datacolumn=datacolumn,
    imagename=imagename, imsize=imsize, antenna="", scan="", cell=cell,
    phasecenter="", reffreq=reffreq, gridder="standard", conjbeams=False,
    mosweight=False, rotatepastep=5.0, pblimit=0.1, deconvolver="mtmfs",
    scales=scales, nterms=2, smallscalebias=0.4, weighting="briggs",
    robust=robust, uvtaper=uvtaper, niter=niter, gain=gain, threshold=0.0,
    nsigma=nsigma, cycleniter=cycleniter, cyclefactor=cyclefactor, usemask=usemask,
    pbmask=pbmask, mask=mask, restart=True, savemodel=savemodel, calcres=calcres,
    calcpsf=calcpsf, stokes=stokes, parallel=parallel)


try:
    hifv_importdata(vis=vis, session=["session_1"])
    hifv_hanning(pipelinemode="automatic")
    hifv_flagdata(quack=False, \
    intents="*POINTING*,*FOCUS*,*ATMOSPHERE*,*SIDEBAND_RATIO*, *UNKNOWN*, *SYSTEM_CONFIGURATION*, *UNSPECIFIED#UNSPECIFIED*", \
    autocorr=True, clip=True, flagbackup=False, fracspw=0.0, tbuff=0.225, \
    hm_tbuff="manual", edgespw=False, template=True, online=True, \
    baseband=False, shadow=True)
    hifv_vlasetjy(pipelinemode="automatic")
    #fill model column for resolved calibrator
    run_tclean_cal_model(vis,"J1442+3234_0.45s_5",field="J1442+3234", calcres=True, calcpsf=True,\
    savemodel="modelcolumn", parallel=False)

    hifv_priorcals(tecmaps=False, swpow_spw="6,14")
    hifv_testBPdcals(pipelinemode="automatic")
    hifv_checkflag(checkflagmode="bpd-vlass")
    hifv_semiFinalBPdcals(pipelinemode="automatic")
    hifv_checkflag(checkflagmode="allcals-vlass")
    hifv_solint(limit_short_solint=0.45)
    run_tclean_cal_model("calibrators.ms","J1442+3234_0.45s_5",field="J1442+3234", calcres=True, calcpsf=True,\
    savemodel="modelcolumn", parallel=False)
    hifv_fluxboot(fitorder=2)

    run_tclean_cal_model(vis,"J1442+3234_0.45s_5",field="J1442+3234", calcres=True, calcpsf=True,\
    savemodel="modelcolumn", parallel=False)

    # CASA commands from hifv_finalcals (casa_commands.log) replacing a setjy call with a run_tclean_cal_model call
    # setjy(vis="finalcalibrators.ms", field="J1442+3234",
    #      spw="2,3,4,5,6,7,8,9,10,11,12,13,14,15,16,17", selectdata=False,
    #      scalebychan=True, standard="manual", listmodels=False,
    #      fluxdensity=[0.33197980349704775, 0, 0, 0], spix=[-0.1780925888250928,
    #      0.11205815765735133], reffreq="2928192670.41Hz", usescratch=True)
    run_tclean_cal_model("finalcalibrators.ms","J1442+3234_0.45s_5",field="J1442+3234", calcres=True, calcpsf=True,\
    savemodel="modelcolumn", parallel=False  )
    # Remaining gaincal calls

    # CASA commands for hifv_circfeedpolcal
    # CASA commands for hifv_flagcal
    # CASA commands for hifv_applycal

    hifv_checkflag(checkflagmode="target-vlass")
    hifv_statwt(pipelinemode="automatic")
    hifv_plotsummary(pipelinemode="automatic")  # does not work properly due to manual CASA commands
finally:
    h_save()
```

# 4 Comparison of Calibration With and Without a Model

The impact of a calibrator model is evaluated by generating 8–10 images from each tile where a calibrator model was utilized during calibration. These images are generated using the standard SE and Quicklook imaging pipelines and we created and compared the images of data where a calibrator model was and was not used.

## 4.1 Comparison of Images

It is necessary to compare the morphology of the sources in the resultant images to determine if there is any impact from using the calibrator model during calibration. We selected bright sources to perform a visual comparison as these sources with high dynamic range are the most likely to exhibit obvious distortions resulting from resolved structure in the complex gain calibrator. Arguably, the most important image comparison is the SE images because they have self-calibration applied, which could compensate for complex gain calibration errors that result from the resolved calibrator, and only the SE images would ever have a calibrator model used in the calibration pipeline in operations. The Quicklook images will always be produced without using a calibrator model. However, the comparison to the Quicklook images is also enlightening because self-calibration is not applied and may more directly show the impact of the calibrator model. We show a comparison of the SE and Quicklook images created from data calibrated with and without a model in Figures 3 and 4 for the tile T08t10 and Figures 5 and 6 for tile T08t07.

There are some extremely subtle differences in the images that are apparent in Figures 3 and 4, but the differences are mostly confined to the low level emission around the bright source, which is already impacted by complex gain errors that are very obvious in the Quicklook image and are reduced—but not fully corrected—in the SE image. The same is also true for the images in Figures 5 and 6; some artifacts look qualitatively better in the image that used a calibrator model (and vice-versa) for both the SE and Quicklook images. Nevertheless, there is no obvious impact on the emission morphology of the bright sources that would motivate us to favor the data calibrated with a model over the standard calibration.

## 4.2 Comparison of Component Catalogs

The lack of an obvious impact on the emission morphology does not preclude systematic effects that could be introduced to the source flux densities, spectral indices, and beam shapes as a result of the spatially-resolved calibrator. Therefore, it is also necessary to examine the measurements made toward the ensemble of sources detected in a given image.

We extracted components from each image using *pyBDSF* as called via the component catalog generation script that is run on the SE continuum images following the SE continuum imaging pipeline. The script also works on the Quicklook images, but ignores the spectral index extraction because the spectral index images are not delivered as a Quicklook product. Then for each image, we match the components identified in the images calibrated with and without a calibrator model with a $0\farcs5$ tolerance. We then generated plots of the quantities: total flux density, peak intensity, spectral index, major axis, minor axis, and position angle, plotting the quantities from the images generated from data with and without a model on each axis. We

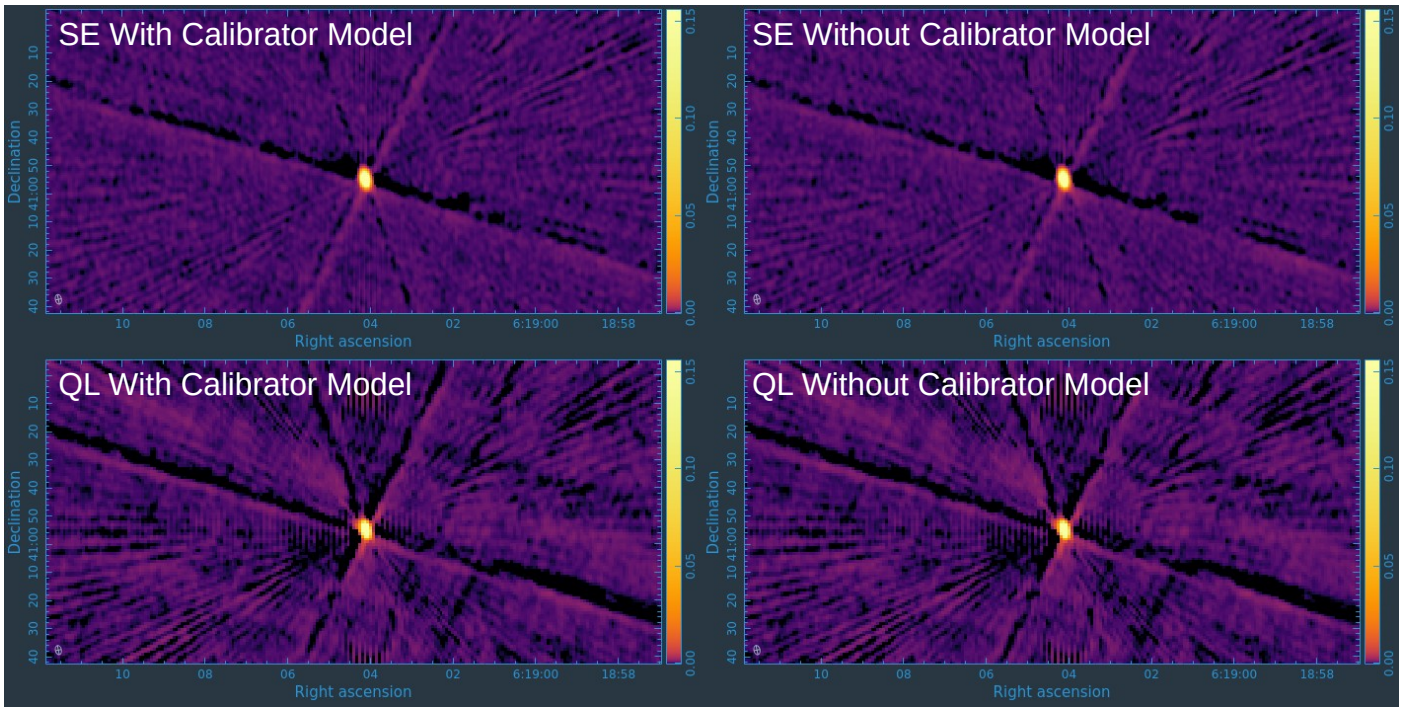


Figure 3: Single Epoch (top) and Quicklook (bottom) images for T08t10.J061820−113000 generated using data calibrated with calibrator model (left) and without a model (right).

then computed histograms of the flux density, peak intensity, and spectral index differences and we fit Gaussians to these histograms to characterize their mean offsets and standard deviations. We performed these evaluations on a per-tile basis since the calibration differences that result from using a calibrator model should systematically affect all the images from a tile. We show the resultant plots for all the Quicklook images in Figure 7 and for all SE images in Figure 8. Then we examine the concentration of the source flux—i.e., the total flux density divided by the peak intensity—for the QL and SE images in Figure 9, and lastly we examine the impact on spectral index in Figure 10. The fitted Gaussian parameters for the distributions of flux density differences and alpha differences in the QL and SE images are also provided in Tables 2 and 3 for quick reference, both overall and per tile.

The Quicklook images show no systematic difference in their total flux density nor their peak intensity as shown in the top panels of Figure 7. The measurements are concentrated around the 1:1 line with very little spread away from the line in both total flux density and peak intensity. There are a small number of large outliers. Inspection of these large outliers reveal them to typically be very near bright sources where the component detection routine is picking up imaging artifacts that can get mismatched and have subtle position shifts between the images generated from data calibrated with and without a model. We conclude that these large outliers are spurious and are not true differences in the images. A Gaussian fit to the flux density histogram in Figure 7 shows that the mean difference between integrated flux density in the images with and without a model is 13.6 $\mu$Jy, with a standard deviation of

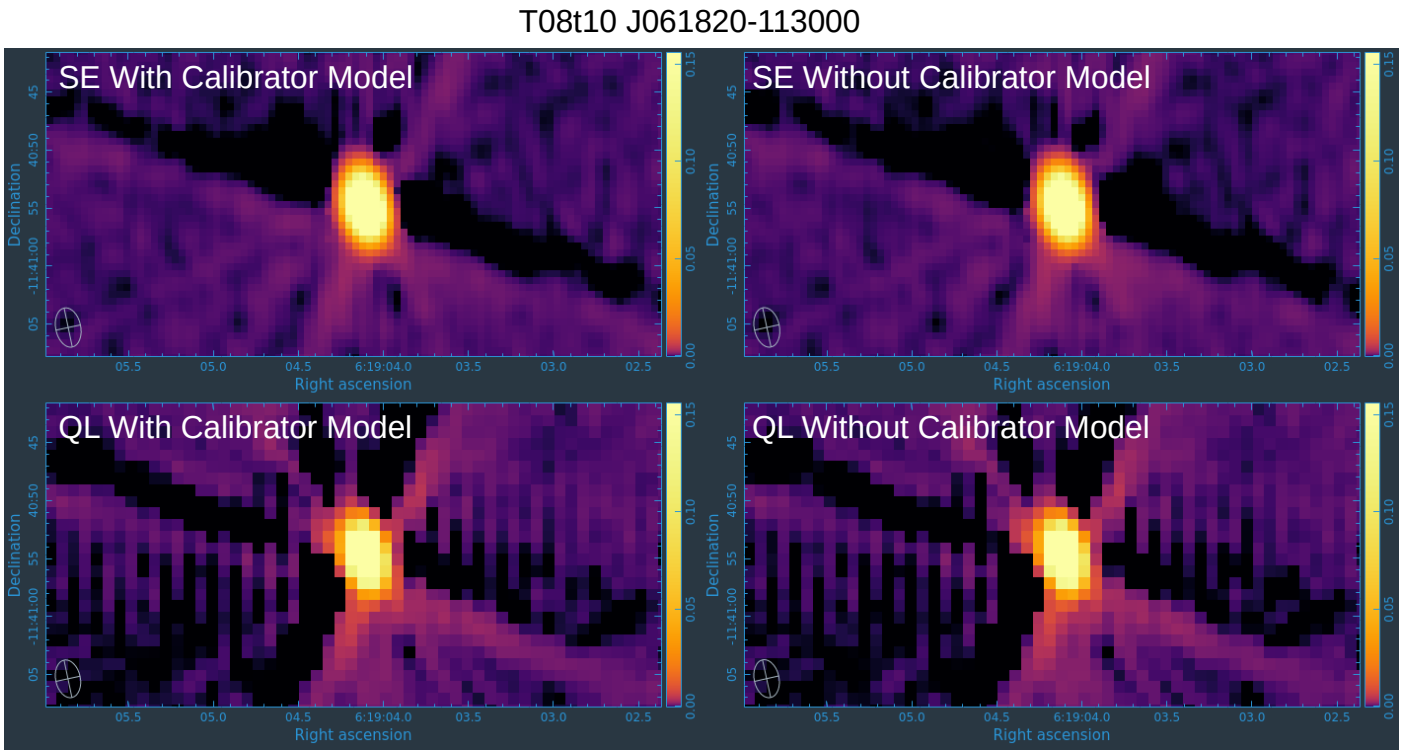


Figure 4: Same as Figure 3, but zoomed-in on the bright source.

68.5$\mu$Jy. The wide skirts apparent in the histograms are the result of the spurious components, as noted previously, and the log scale over-emphasizes these outliers. The mean offsets of the distributions are quite small and far below the typical VLASS image RMS noise of 150 $\mu$Jy. The average offset between the peak intensities is of a similar magnitude, but the integrated flux density has a positive offset while the peak intensity has a negative offset.

The results from the SE images are very similar for the Quicklook images as shown in Figures 8 and 10. Like the Quicklook flux density distributions, there are some large outliers, but those outliers are also the result of image artifacts. The peak intensity scatter plot appears very similar to the total flux density scatter plot. The histograms reveal that there are offsets in the integrated flux density distribution of 5.8 $\mu$Jy and $-12.4$ $\mu$Jy in peak intensity. These offsets are similar in magnitude to what was observed in the Quicklook data and are still well below the typical RMS noise in VLASS images. Indeed the standard deviations of the distributions are less than the RMS noise of VLASS images.

The distributions of total flux density divided by peak flux intensity, shown in Figure 9 for both the QL and SE images, are entirely consistent with each other. If the resolved calibrator was negatively impacting the source morphology we would expect to see a difference in the distributions between those calibrated with and without a model. Instead, as we saw from the comparison of the images, the use of a calibrator spatial model does not impact the ratio of total flux density to peak intensity. We note that the tile T04t34 does have distributions shifted to slightly larger (but statistically significant) values relative to other tiles (the distributions with and without a model for T04t34 are statistically identical). The overall shift of the distribution

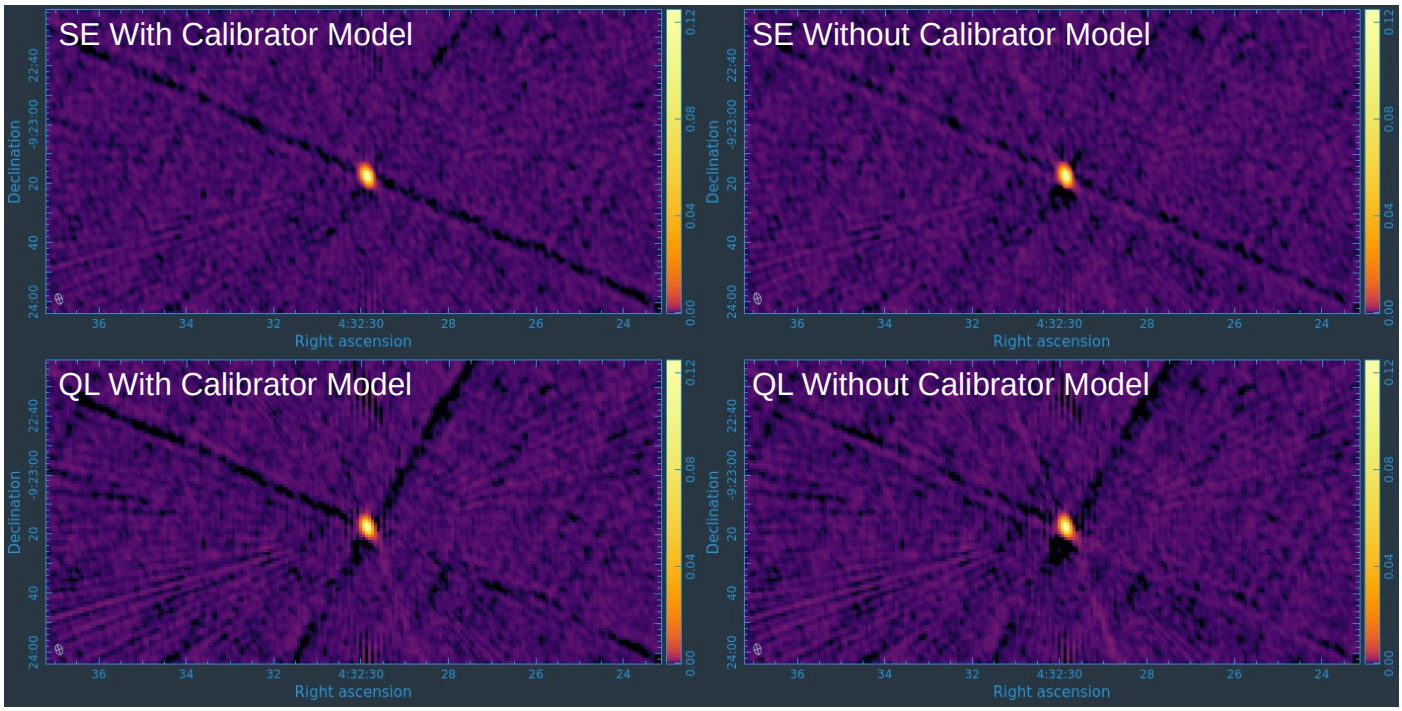


Figure 5: Single Epoch (top) and Quicklook (bottom) images for T08t07.J043425−0930003 generated using data calibrated with calibrator model (left) and without a model (right).

peak toward larger total/peak relative to other Tiles can be attributed to the use of the mosaic gridder for producing the images and low declination of this tile (and hence high zenith angle); see VLASS Memo #17.

Finally, the comparison of the spectral index in Figure 10 shows that the typical values for the identified components are very similar between the images, with most points clustered around the 1:1 line. The histogram of spectral index differences shows that over all tiles the mean offset is 0.033, with a standard deviation of 0.141. The expected uncertainty in spectral index is ∼0.2 when using the mosaic gridder, so this distribution is in line with the expected uncertainties. The standard deviation of the overall distribution is slightly larger than that of the individual tiles due to spread in the systematic offsets between the different tiles.

Table 2. QL Tile Comparisons

| Tile | QL Flux density offset ($\mu$Jy) | QL Peak offset ($\mu$Jy/beam) | Total/Peak Center (Model, no Model) |
|---|---|---|---|
| T04t34 | 72.5±0.6 (117.7±0.6) | −49.0±0.2 (60.8±0.2) | 1.28±0.04, 1.19±0.03 |
| T08t07 | 39.0±0.2 (72.5±0.2) | −15.3±0.1 (44.3±0.1) | 1.07±0.03, 1.04±0.02 |
| T08t10 | −9.2±0.2 (58.6±0.2) | −15.8±0.1 (30.6±0.1) | 1.08±0.03, 1.08±0.02 |
| T14t15 | 10.4±0.1 (54.7±0.1) | −10.9±0.04 (30.2±0.04) | 1.09±0.02, 1.09±0.02 |
| Overall | 13.6±0.2 (68.5±0.2) | −15.1±0.1 (35.6±0.1) | 1.10±0.03, 1.10±0.02 |

The values shown in parentheses are the standard deviations of the distributions.

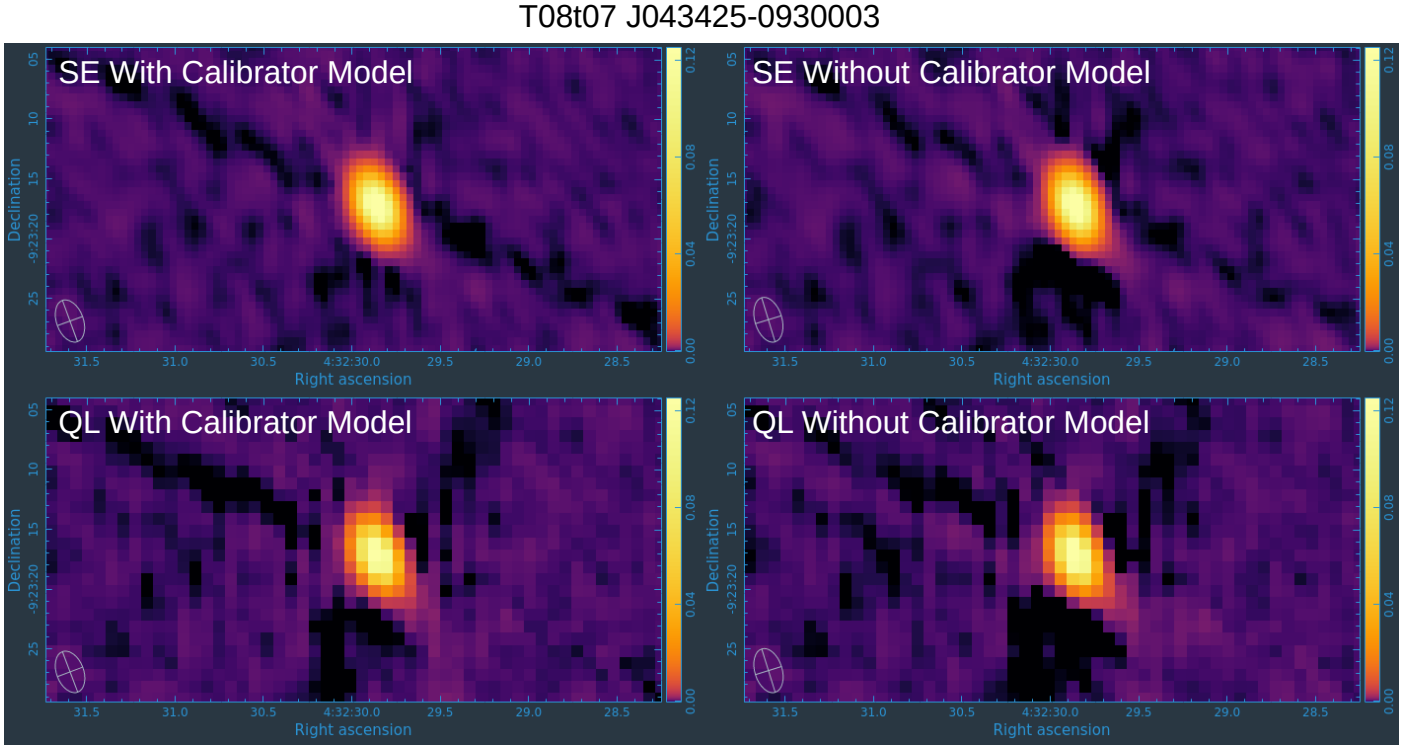


Figure 6: Same as Figure 5, but zoomed-in on the bright source.

Table 3. SE Tile Comparisons

| Tile | SE Flux density offset ($\mu$Jy) | SE Peak offset ($\mu$Jy/beam) | SE Alpha offset | Total/Peak Center (Model, no Model) |
|---|---|---|---|---|
| T04t34 | 27.5±0.5 (94.6±0.4) | −33.5±0.2 (59.9±0.2) | 0.045±0.002 (0.091±0.002) | 1.19±0.04, 1.18±0.03 |
| T08t07 | 30.1±0.3 (104.3±0.3) | −14.8±0.1 (56.5±0.1) | 0.073±0.002 (0.09±0.002) | 1.06±0.01, 1.03±0.01 |
| T08t10 | −12.8±0.3 (82.3±0.2) | −15.8±0.1 (39.8±0.1) | −0.065±0.002 (0.112±0.002) | 1.08±0.02, 1.08±0.02 |
| T13t13 | 16.8±0.2 (74.5±0.2) | −9.8±0.1 (35.5±0.1) | 0.028±0.002 (0.09±0.002) | 1.10±0.03, 1.05±0.06 |
| T13t15 | 5.8±0.2 (75.9±0.2) | −6.6±0.1 (42.5±0.1) | 0.014±0.002 (0.09±0.002) | 1.11±0.02, 1.11±0.02 |
| T14t15 | 8.1±0.2 (80.2±0.02) | −7.1±0.1 (42.0±0.1) | 0.031±0.001 (0.07±0.001) | 1.08±0.02, 1.07±0.02 |
| Overall | 8.5±0.2 (85.0±0.02) | −12.0±0.1 (44.2±0.1) | 0.0184±0.002 (0.12±0.002) | 1.10±0.02, 1.09±0.02 |

The values shown in parentheses are the standard deviations of the distributions.

# 5 Conclusions and Recommendation to the VLASS Project

Overall, the images created from data calibrated with and without a calibrator model show only minor differences. These differences do not significantly impact the apparent source morphology in a visual comparison. Moreover, quantitative measurements of component properties extracted from the images also do not show significant differences in total flux density, peak intensity, or spectral index. Thus, the quantitative differences that result from aggregate measurements of components do not indicate that calibration with a model results in a substantive difference from calibration without a model. We note, however, that all the resolved calibrators used by VLASS were dominated by a bright central component that was well-centered. The central component was >10× the flux density of any secondary components and therefore the gain solvers implicitly using a point source model were not providing pathological results

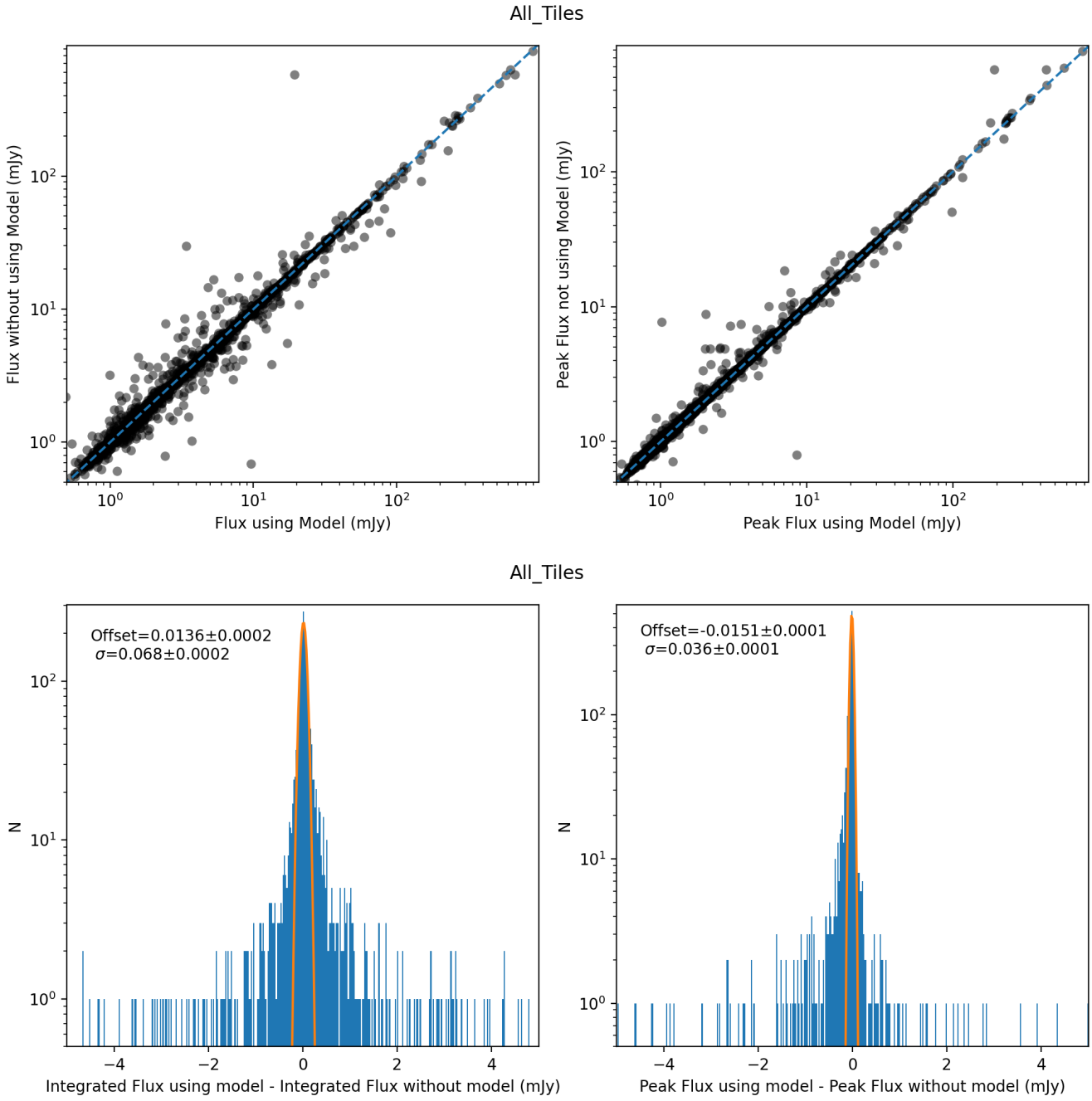


Figure 7: Comparison of flux density measurements made with and without models using Quicklook images for the integrated flux densities (left) and peak intensities (right). The top panels show the measured flux densities plotted against each other, with the 1:1 line drawn as the dashed blue line. The bottom panels show histograms of the differences between the measurements with and without a model. The orange curve is a Gaussian fit to the distribution with its mean and standard deviation annotated in the top left of each panel.

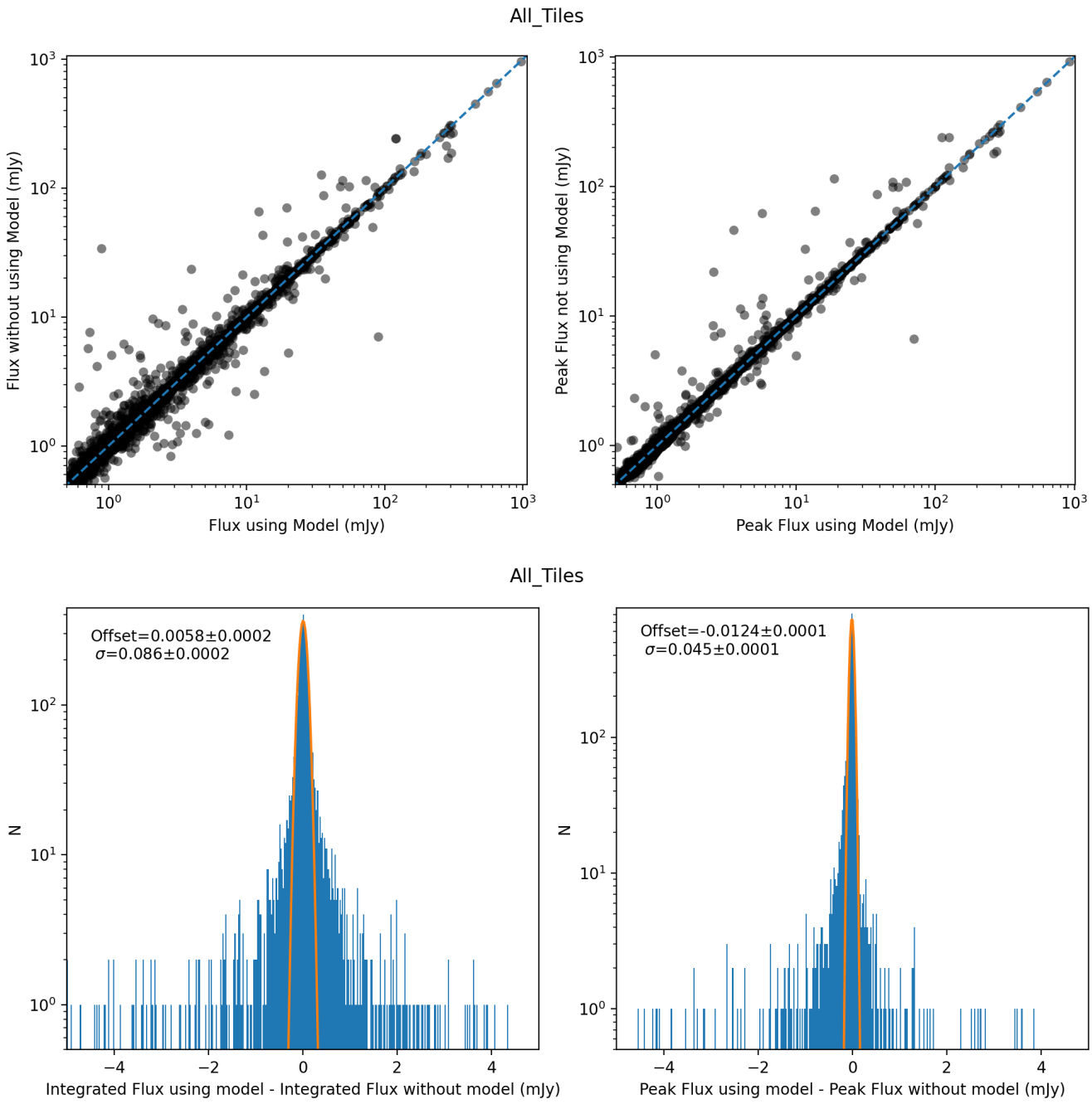


Figure 8: Same as Figure 7 but for the Single Epoch images.

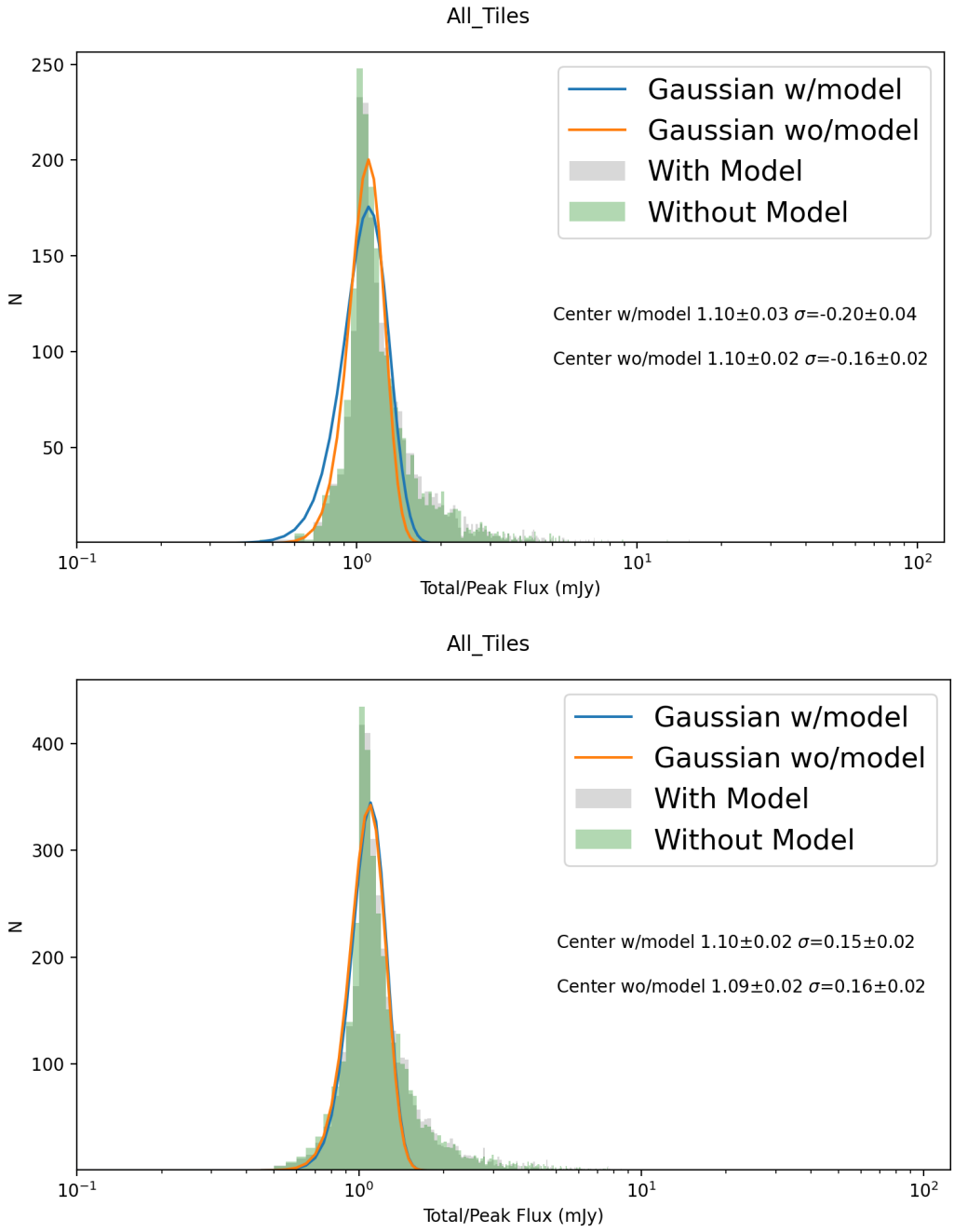


Figure 9: Histograms of total flux density divided by the peak intensity for the QL images (top) and the SE images (bottom).

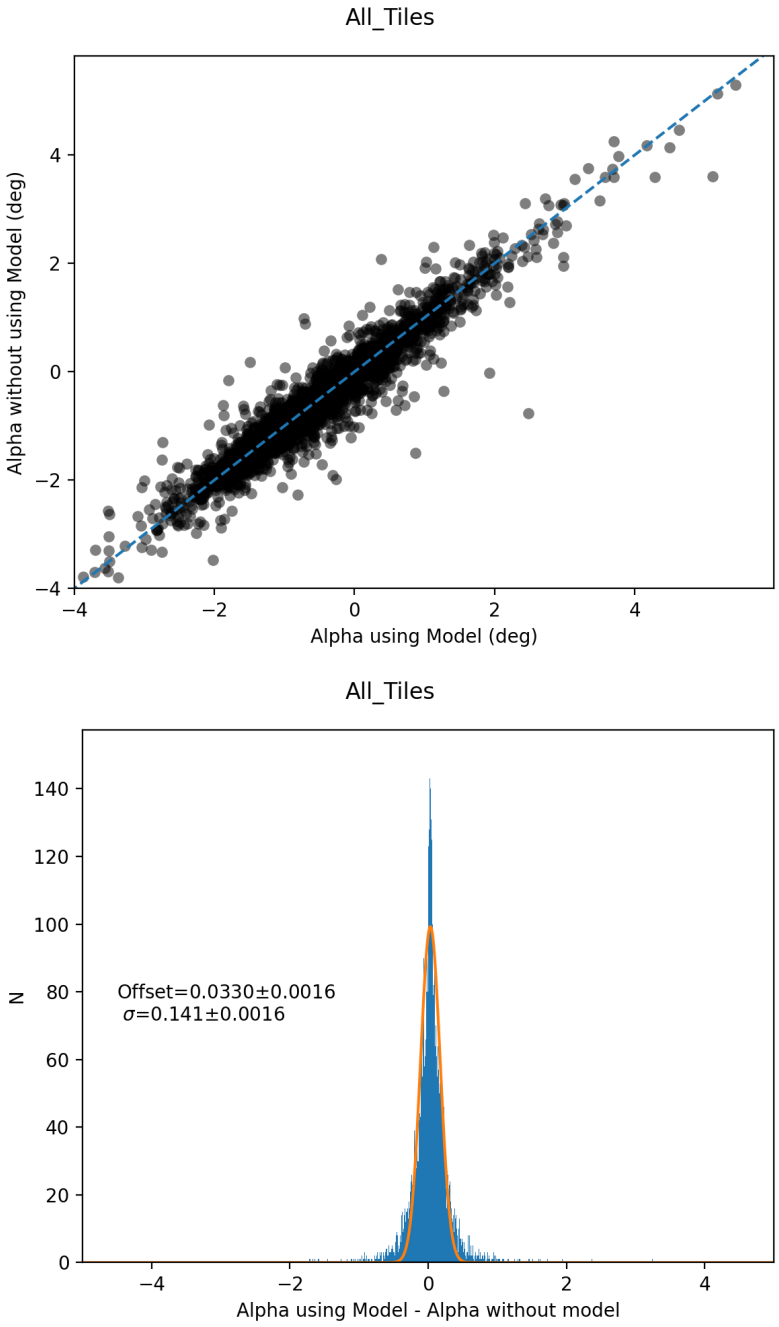


Figure 10: Comparison of spectral index measurements made with and without models using Single Epoch images. The top panel shows the measurements plotted against each other with the 1:1 relation drawn as the dashed blue line. The bottom panel shows the histogram of the differences with the Gaussian fit to the distribution overlaid as the orange curve and the parameters annotated at the left.

that could occur if there were multiple co-equal components. *Thus, the results of this memo specifically apply to the calibrators used in the VLASS survey and not all resolved calibrators that might be used in standard VLA observations.*

This memo demonstrates the feasibility of both model creation and the calibration of VLASS (and VLA) data using a spatial model for a complex gain calibrator, and where in the pipeline changes would be necessary to make use of a calibrator spatial model. However, the results from this memo do not demonstrate the necessity of using a calibrator model for VLASS data that used calibrators having spatially-resolved structure.

From a perspective of best practices, it would be better to calibrate the VLASS data using a spatial model when the data were taken using a resolved calibrator. However, significant effort would be required by the VLASS team to create calibrator models for the resolved calibrators and development would be required to support the use of models in the pipeline. The analysis presented does not indicate that there is a tangible scientific benefit to calibrating with a model. Therefore, we conclude that the VLASS project does not require the use of calibrator models to meet the science requirements of the survey and recommend that the project does not dedicate effort to making use of calibrator models in the pipeline.

# 6 Acknowledgments

We wish to acknowledge the efforts by Josh Marvil to characterize the calibrator structure in VLASS data and his early contributions to the calibrator modeling effort. We also acknowledge useful discussions with Juergen Ott, Mark Lacy, Steve Myers, and Jeff Kern.